Study of strain localizations in a polycrystalline medium in presence of a quasi-static crack

L. Patriarca, P.G. Luccarelli, S. Foletti

Politecnico di Milano, Department of Mechanical Engineering, via La Masa 1, 20156, Milano, Italy
luca.patriarca@polimi.it, pietrogiovanni.luccarelli@polimi.it, stefano.foletti@polimi.it

ABSTRACT. Numerical techniques have been widely applied in many recent works to investigate micro-scale behavior of materials. This work focuses on the analysis of strain localizations in a Nickel-based alloy, Haynes 230. Numerical models and experiments concern the study of the strain field generated around the crack tip inside a polycrystalline medium when the crack is quasi-static (not propagating). Experimentally, the tests were conducted in load control; one face of the specimens was monitored by high-resolution Digital Image Correlation (DIC) technique to evaluate the strain field ahead of the crack tip. The simulations were conducted adopting an open source finite element code, Warp3D, which implements a state of art Crystal Plasticity (CP) model. The models of the polycrystalline matrix were created considering the data obtained inspecting the specimen surface by the Electron Back-Scatter Diffraction (EBSD) technique, which allowed defining grains size and orientations. Experimental and numerical results were then compared in terms of strain localizations to evaluate the prediction capabilities of the models. The comparison focused on strain field extension and active grains.

KEYWORDS. Crystal Plasticity; Digital image correlation; Polycrystalline aggregate.

INTRODUCTION

In the last two decades, crystal plasticity finite element (CPFE) methods have evolved creating a link between the theoretical studies on the micro-mechanics of materials and the continuum field of deformation theories. CPFE are currently used to model several micro-mechanisms of deformation (slip, twinning, grain boundaries interaction, etc.) which cover a wide range of applications. CPFE are currently also adopted to fractured polycrystalline, especially when the cracks are small compared to the grain size, by Rice [1-3]. Recently, other studies focused on simulated crack propagation in single crystals [4-5] provided estimations of crack opening levels in comparison with experimental results. On the other

hand, studies on stationary and propagating cracks in polycrystalline material is still an open field where many contributions [6-7] focused primarily on the effects of strain field transmission across grain boundaries. The adoption of Voronoi structures was used to study the effect of a stationary crack in a C(T) polycrystalline specimen [8], the results pointed to analyze the heterogeneity of stress and strain fields acting at the crack tip.

Most of the works related to CPFE modeling consider random generated structures and use experiments for macro-scale comparisons. A link between Crystal Plasticity (CP) simulations and experiments at meso-scale and micro-scale is still an open field of research. Surface localizations can be nowadays performed at sub-grain scales by Digital Image correlation (DIC) and subsequently compared with the CPFE results to have a feedback on the predictive capabilities of the models. In the current work, simulations and experiments were conducted on a Nickel based super-alloy, Haynes 230 [9]. The study of nickel-based super-alloys is increasing through the years as these materials show high mechanical properties and excellent resistance to corrosion at high temperatures. The present analysis was performed on a single notched polycrystalline specimen which was pre-cracked in compression. The investigation concerns the study of the residual strain field generated at the tip of a quasi-static crack. Grain orientation and geometry were detected by Electron Backscatter Diffraction (EBSD) technique. Concurrently, the experimental evaluation of the strain field was performed adopting high resolution sub-grain DIC strain measurements.

Numerically, the CPFE simulations were conducted considering the real geometry of the specimen and adopting a CP algorithm implemented in Warp3D [10]: this code allows to represent the material behavior at the grain scale thanks to the adoption of physical and kinematics models, which for FCC materials, like Ni-based super-alloy, associate the plastic deformations mainly to dislocation motion according to the active slip systems.

In the following sections are presented the adopted CP model, the CP parameters identification for the investigated alloy and finally the experimental procedure and the simulations involving the quasi-static crack.

CRYSTAL PLASTICITY MODEL

The mechanical behavior of grains can be modeled with an elastic-plastic model where the crystals' kinematics is considered as a combination of dislocation motion, rotation of the crystalline matrix and elastic deformation [7,11].

The deformation gradient multiplicative decomposition can be written as [12]:

$$F = F^e F^p \qquad (1)$$

where F is the deformation gradient, F^e and F^p are, respectively, its elastic and plastic components. By the analysis of these gradients it is possible to obtain the formulation for the objective stress function which needs to be integrated by the finite element solver [13]. To solve the problem, the definition of an hardening rule is required in the formulation of the slip rate along the slip plane (s):

$$\dot{\gamma}^{(s)} = \frac{\dot{\gamma}_0}{\tilde{\tau}} \left| \frac{\tau^{(s)}}{\tilde{\tau}} \right|^{n-1} \tau^{(s)} \qquad (2)$$

where $\dot{\gamma}_0$ is a reference strain rate, $\tau^{(s)}$ is the resolved shear stress, n is the exponent of the slip rate, $\tilde{\tau}$ is the shear strength which requires the definition of the hardening model.

The hardening law, originally proposed in [14] by Follansbee and Kocks, implemented in Warp3D has the following expression:

$$\tilde{\tau}\left(T,\dot{\varepsilon}_p\right) = \hat{\tau}_a + \frac{\mu}{\mu_0} \tilde{\tau}_y\left(T,\dot{\varepsilon}_p\right) + \frac{\mu}{\mu_0} \overline{\tau}\left(T,\dot{\varepsilon}_p\right) \qquad (3)$$

The shear strength $\tilde{\tau}$ is temperature and rate dependent; $\hat{\tau}_a$ is the athermal and rate-independent component influencing the yield strength; $\tilde{\tau}_y$ is the thermal and rate dependent component of the yield strength; $\overline{\tau}$ accounts for the work

hardening; μ is the shear modulus and μ_0 is a reference value. The expression for the evolution of $\bar{\tau}$ relies on a Voce type law:

$$\dot{\bar{\tau}}\left(T,\dot{\varepsilon}_p\right) = \vartheta_0 \left[1 - \frac{\bar{\tau}\left(T,\dot{\varepsilon}_p\right)}{\tilde{\tau}_v\left(T,\dot{\varepsilon}_p\right)} \right] \sum_{s=1}^{n_s} \dot{\gamma}^{(s)} \tag{4}$$

In Eq. (4) ϑ_0 is the initial slope of the work hardening curve (in a $\tilde{\tau}$ vs. ε_p plot); n_s is the number of possible slip systems (s); $\tilde{\tau}_v$ is the work hardening saturation strength. The definition of $\tilde{\tau}_y$ and $\tilde{\tau}_v$ rely on an Arrhenius type equation [15]:

$$\tilde{\tau}_i\left(T,\dot{\varepsilon}_p\right) = S_i\left(T,\dot{\varepsilon}_p\right)\hat{\tau}_i = \left[1 - \left(\frac{kT}{g_{0,i}\mu b} \ln \frac{\dot{\varepsilon}_{0,i}}{\dot{\varepsilon}_p} \right)^{1/q_i} \right]^{1/p_i} \hat{\tau}_i \tag{5}$$

Where S_i is a scale factor and $\hat{\tau}_i$ is a constant for the saturation strength; k is the Boltzman constant; b is the magnitude of the Burgers vector; $g_{0,i}$ is the activation energy; $\dot{\varepsilon}_{0,i}$ is a reference strain rate; p_i and q_i are statistical constants.

PARAMETERS IDENTIFICATION

According the Eqs. (3)-(5), there are 16 unknown parameters which are required to be determined for the specific investigated alloy in order to perform the CP simulations. To identify the constants a tensile test was considered. The fitting of the tensile stress-strain curve, following the trial and error procedure, gave an estimation of the CP parameters (Tab. 1).

The model used for this simulation was created starting from an EBSD scan of the specimen area showed in Fig. 1. This polycrystalline model was constructed to reproduce the real condition of the experiment, which was in displacement control.

Fig. 1a shows the geometry of the tested specimen with a focus on the extracted area which was modeled with CP material. The entire model counts about 12000 linear hexahedral elements distributed over an area of 0.722 mm by 0.702 mm and a thickness of 0.04 mm. The model includes over 700 grains which were modeled columnar through the thickness. The simulation of the tensile test was carried out imposing a displacement to the upper surface of the volume and modeling a double symmetry on the other two surfaces.

E	v	μ_0	b	$\hat{\tau}_a$	$\hat{\tau}_y$	$g_{0,y}$	q_y
195 GPa	0.33	80 GPa	3.5e-7 mm	0 MPa	120 MPa	2.37	1.8
p_y	$\dot{\varepsilon}_{0,y}$	$\hat{\tau}_v$	$g_{0,v}$	q_v	p_v	$\dot{\varepsilon}_{0,y}$	ϑ_0
0.9	1e10 s^{-1}	65 MPa	1.6	0.34	0.5	1e7 s^{-1}	24000 MPa

Table 1: Mechanical Threshold Stress model's parameters identified by the tensile test simulation.

The results in terms of stress-strain curves are shown in Fig. 1b: it is possible to observe a good agreement between the predicted tensile curve and the experimental one adopting the parameters listed in Tab. 1.

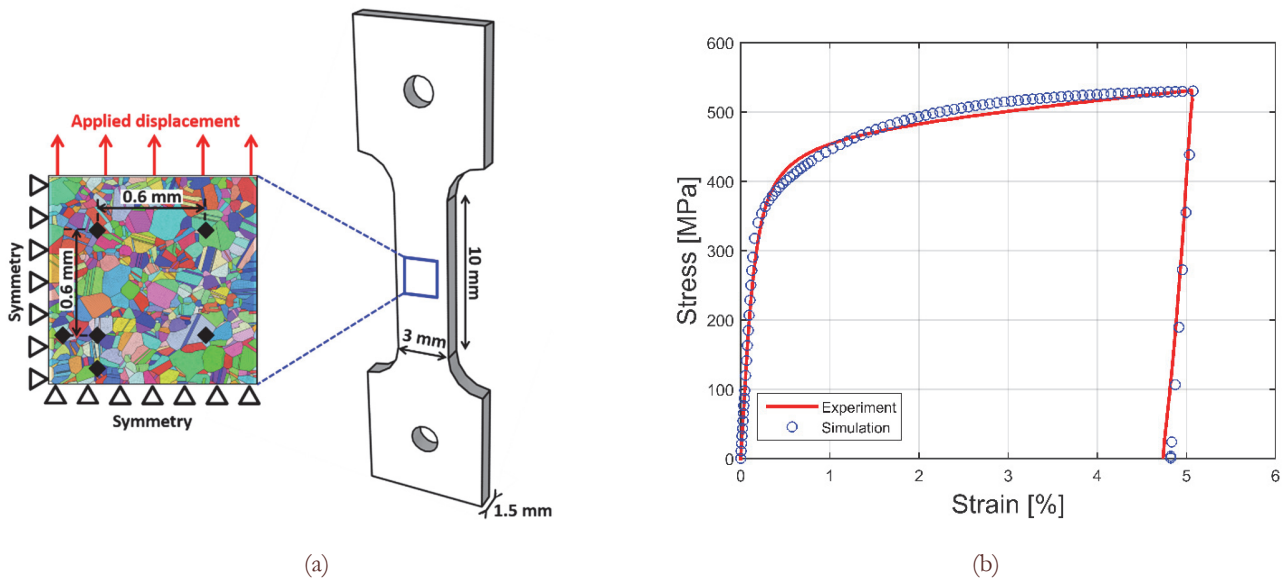(a)   (b)

Figure 1: Tensile test analysis: (a) Geometry of the dog-bone specimen used for the test and the area simulated by crystal plasticity algorithm; (b) Comparison between the experimental and numerical stress strain curves after material parameters optimization.

Model's prediction was also compared in terms of strain distribution at the unloading condition. Fig. 2 shows the histogram of the strain occurrence over the inspected area between the DIC strain measurements and the CP simulation. The comparison shows the capability of the model to capture the strain distribution trend, with a good approximation of the mean value: 4.83 % for the experiment and 4.92% for the simulation.
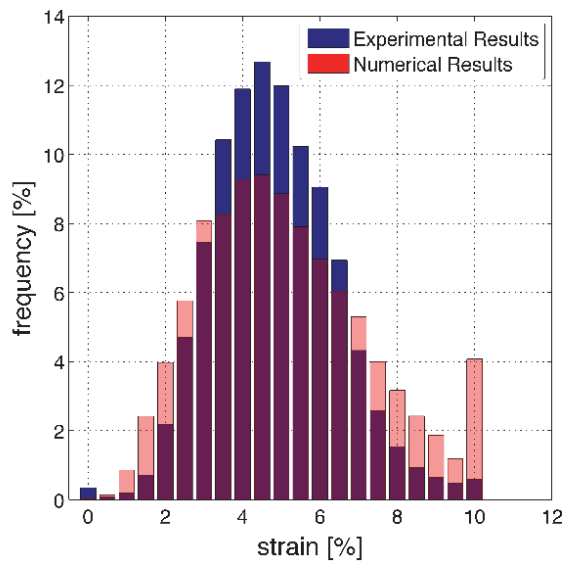

Figure 2: Histogram showing the comparison of the strain fields detected by DIC and simulation of the tensile test.

QUASI-STATIC CRACK – EXPERIMENTAL PROCEDURE

The setup of the test was constructed with the aim to capture, over a wide surface of the material, the localization of deformation around the crack tip. The geometry of the specimen, Fig. 3b, was chosen according to the 4 pins grips for Deben micro-testing machine, Fig. 3a. The notch of 0.5 mm was produced by electrical discharge machining. The nominal dimension of the net section of the specimen is 6 mm x 2 mm, while the specimen gauge length is 15.5 mm.
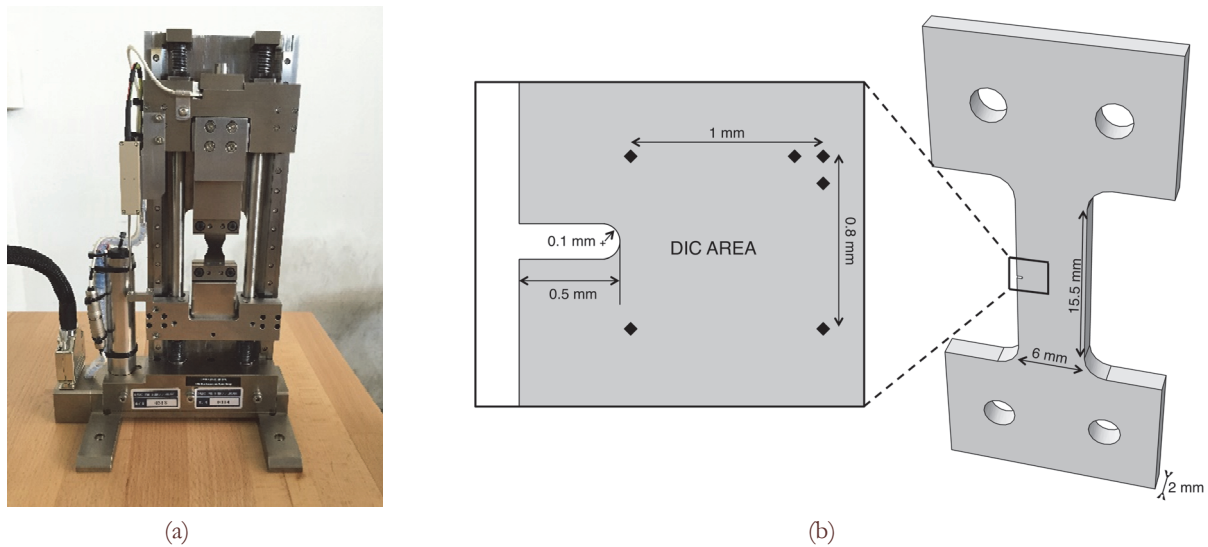
Figure 3: Experimental setup: (a) Deben Micro-Testing Machine, 5 kN dual leadscrew; (b) Specimen geometry and micro-indentation markers.

The specimen was initially polished with abrasive SiC paper, diamond suspension and colloidal silica. Successively, a rectangular region of 1 mm x 0.8 mm was selected in front of the notch and marked with micro-indentations. An EBSD map was then performed in the marked region in order to precisely establish the grains orientation and geometry in the specimen region. According to preliminary plastic radius calculations, the selected EBSD region is large enough to contain the strain localization produced around the crack tip.

The specimen was successively pre-cracked in compression in order to limit the load history effects produced by the classical pre-cracking methodologies based on tensile loading cycles. The compressive applied load range was 2700 N (between -3000 N and -300 N), this condition ensured a plastic radius at the notch of about 100 μm. Fig. 4 shows the outcome of the pre-cracking procedure, a crack with a length of 60 μm from the notch was detected.
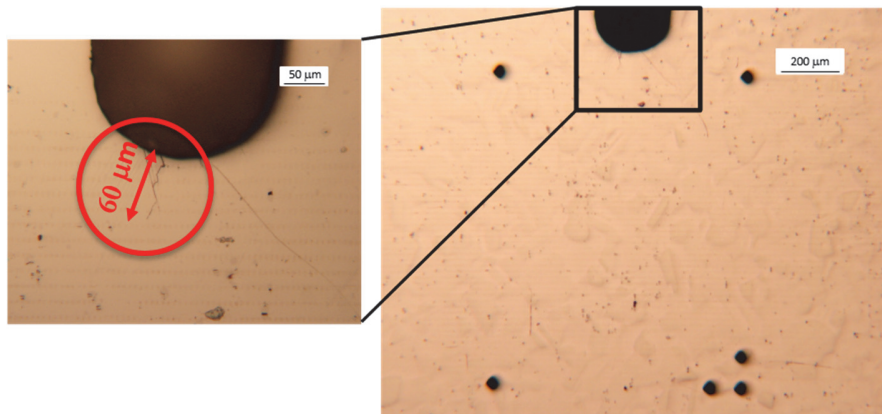

Figure 4: Crack nucleated at the notch tip after the compression pre-cracking process.

Following compression pre-cracking, the specimen was prepared for high resolution ex-situ DIC. A fine speckle pattern was applied to the target surface and enabled to acquire images with a resolution of 0.34 μm/pixel. The images were captured before and after deformation in the un-loaded condition by means of a Carl Zeiss Axio Cam A1 optical microscope. The resulting residual strain field were then overlapped with the EBSD grain map using the micro-indentations as reference points. Finally, the test was performed under a Deben Micro-Testing Machine (maximum load 5 kN, Fig. 3) in load control imposing a load/unload procedure to an objective stress intensity factor of about 20 MPa$\sqrt{m}$. The result of the correlation is shown in Fig. 5; the analysis of the DIC image pointed out the presence of a secondary

crack, which was not visible in Fig. 4. The secondary crack is emanating from the right side of the notch; its length is 40 µm and its effect will be considered in the following models.
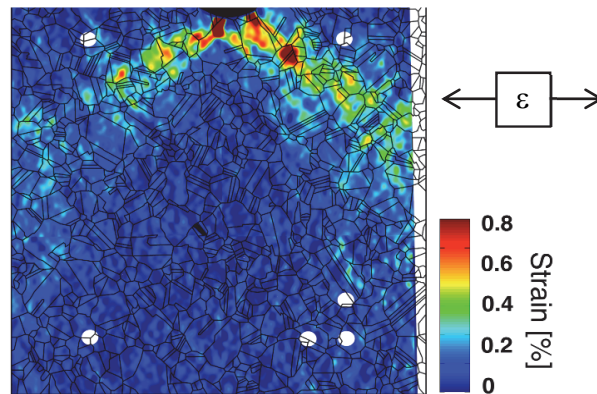

Figure 5: Residual strain field at crack tip measured by Digital Image Correlation.

QUASI-STATIC CRACK - FINITE ELEMENT ANALYSIS

The characterization of the model shown in Fig. 6 required the adoption of some hypotheses:

1. The volume modeled by CP material is confined around the notch and reproduces the EBSD scan information;
2. The remaining volume of the specimen is modeled as purely elastic: its main purpose is to transfer the displacement field generated by the remote applied loading/boundary conditions to the CP portion of material. This hypothesis is acceptable since plastic deformations are confined around the notch;
3. The geometry of the grains in the thickness was considered columnar;
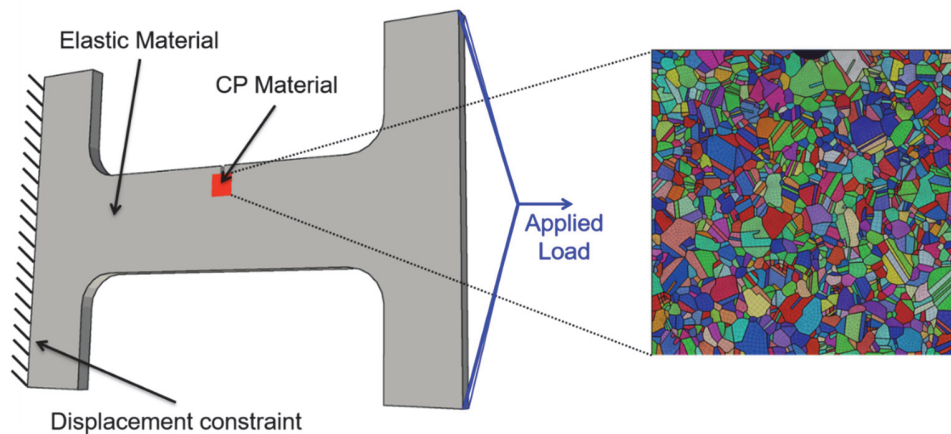4. The primary crack first, and the secondary one later, were modeled as uniform through the thickness.

Figure 6: Model of the quasi-static crack experiment: definition of the loading condition and constraints. Focus on the area modeled by crystal plasticity.

Fig. 6 shows loading and constraint configurations: the load was applied as a force to one node whose displacements were coupled to all nodes belonging to the loaded surface; the opposing face of the specimen was fully constrained in displacement. Finally, Fig. 6 focuses on the details of the CP area modeled and the mesh; here grains geometry and orientations derive from the EBSD. The model, in the CP volume, counts about 1230 grains; they were modeled by 235000 linear hexahedral elements, out of the 350000 of the whole model.
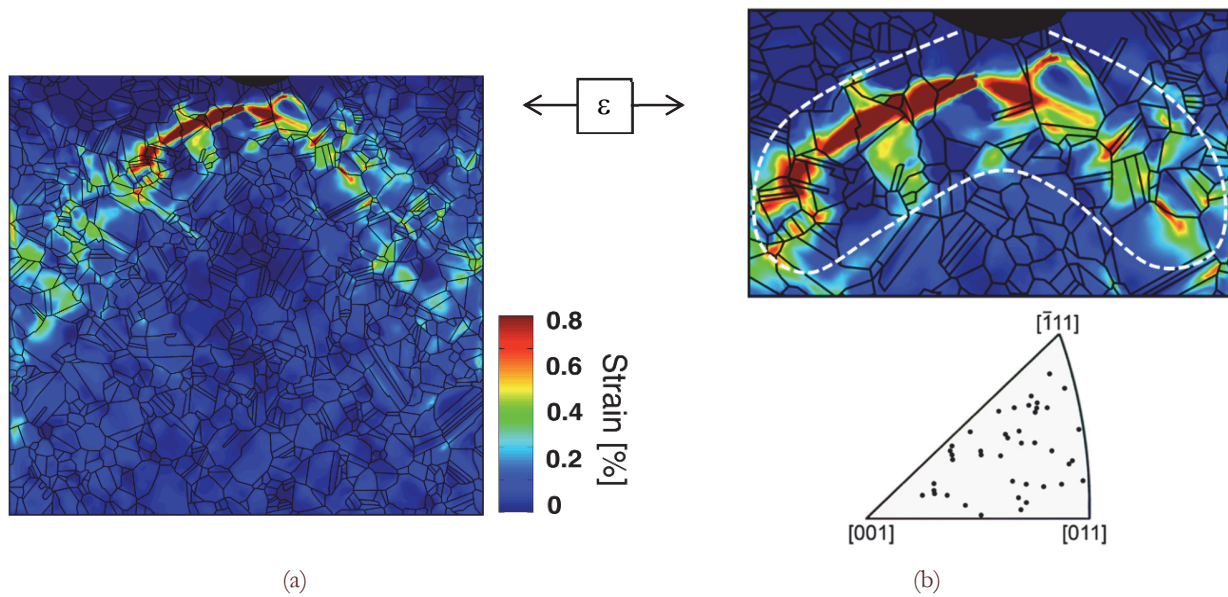
Figure 7: Simulation results of the residual strain field: (a) strain field over the whole crystal plasticity area; (b) focus on the area close to the notch and identification of the crystallographic orientations of the grains showing average local deformations higher than $\varepsilon = 0.2\%$.

The model was loaded to reproduce the experimental conditions where the crack was loaded to reach a nominal stress intensity factor of 20 MPa√m. Fig. 7a shows the results of the simulation in terms of the extension of the residual strain field generated at the crack tip. Focusing on the crack tip region (Fig. 7b), the grains showing average strain localization higher than $\varepsilon = 0.2\%$ were selected (those contained in the area delimited with the white dashed contour). Fig. 7b also shows the crystallographic orientations of the selected active grains in the stereographic triangle. The main outcome of this analysis is that those grains showing high plastic deformations do not have a preferential texture, while the crack tip singularity dictates the deformation.

The main result coming from the simulations, if compared with the DIC, is the agreement with the extension of the strain field. In addition, most of the grains with active slip systems are reproduced. The main difference with DIC is the presence of high concentrated strains at the crack tip. This feature may be related to the hypothesis made of considering the crack front extended through the thickness, while compression pre-cracking usually involves only the surface regions of the specimen.

Another important point of discussion is the approximation introduced with the definition of the CPFE model. The EBSD map characterizes the grain orientation and morphology at the observed surface, but no microstructural information are available along the thickness of the specimen. The CPFE model is then reconstructed extruding the 2D EBSD map, this represents an approximation of the real material microstructure. Studies on 3D grain geometries [16] showed that differences may occur in surface localizations. These differences may affect simulations results while reproducing material behavior under cyclic test, where no discontinuities like cracks, are included and the strain filed is mainly influenced by crystals' orientations and geometries. The introduction of discontinuities localizes the deformation in confined areas and the 3D structure of the grains assume a secondary role in the prediction of the deformation field.

CONCLUDING REMARKS

The proposed work presents the preliminary results obtained by simulating a stationary crack inside a polycrystalline aggregate with a crystal plasticity model. The simulation was successively compared with the experimental observations obtained by means of digital image correlation. This result was achieved reproducing a quasi-static test where the crack was statically loaded. The analysis of the residual strain field shows a good agreement on the extension of the localizations area. Moreover, the study shows that the crack tip stress singularity dictates the deformation of the surrounding grains without preferential orientations.

REFERENCES

[1] Rice, J.R., Inelastic constitutive relations for solids: an internal-variable theory and its application to metal plasticity, JMPS, 19 (1971) 433-455.

[2] Flouriot, S., Forest, S., Cailletaud, G., Köster, A., Rémy, L., Burgardt, B., Gros, V., Mosset, S., Delautre, J., Strain localization at the crack tip in single crystal ct specimens under monotonous loading: 3d finite element analyses and application to nickel-base superalloys, Int. J. Frac., 124 (2003) 43-77.

[3] Potirniche, G.P., Daniewicz, S.R., Analysis of crack tip plasticity for microstructurally small cracks using crystal plasticity theory, Eng. Fract. Mech., 70 (2003) 1623-1643.

[4] Bouvard, J.L., Chaboche, J.L., Feyel, F., Gallerneau, F., A cohesive zone model for fatigue and creep–fatigue crack growth in single crystal superalloys, Int. J. Fatigue, 31 (2009) 868-879.

[5] Rabbolini, S., Luccarelli, P.G., Beretta, S., Foletti, S., Sehitoglu, H., Near-tip closure and cyclic plasticity in Ni-based single crystals, Int. J. Fatigue, 89 (2016) 53-65.

[6] Gall, K., Sehitoglu, H., Kadioglu, Y., Fem study of fatigue crack closure under double slip, Ac. Mat., 44 (1996) 3955-3965.

[7] Potirniche, GP and Daniewicz, SR and Newman, JC, Simulating small crack growth behavior using crystal plasticity theory and finite element analysis, Fatigue Fract. Eng. Mater. Struct., 27 (2004) 59-71.

[8] Lin, B., Zhao, L.G., Tong, J., A crystal plasticity study of cyclic constitutive behavior, crack-tip deformation and crack-growth path for a polycrystalline nickel-based superalloy, Eng. Fract. Mech., 78 (2011) 2174-2192.

[9] Furrer, D., Fecht, H., Ni-based superalloys for turbine discs, JOM, 51 (1999) 14–17.

[10] Healy, B., Gullerud, A., Koppenhoefer, K., Roy, A., Roy-Chowdhury, S., Petti, J., Walters, M., Bichon, B., Cochran, K., Carlyle, A., Messner, M.C., Dodds, R.J., WARP3D: 3-D dynamic nonlinear fracture analyses of solids using parallel computers, Structural Research Series (SRS 607) UILU-ENG-95-2012, University of Illinois at Urbana-Champaign, (2015).

[11] Rice, J.R., Hawk, D.E., Asaro, R.J., Crack tip fields in ductile crystals, Int. J. Fract., 42 (1998) 301-321.

[12] Lee, E.H., Elastic-plastic deformation at finite strains, J. App. Me., 36 (1969) 1-6.

[13] Messner, M.C., Beaudoin, A.J., Dodds, R.J., Consistent crystal plasticity kinematics and linearization for the implicit finite element method, Eng. Co., 32 (2015) 1526-1548.

[14] Follansbee, P.S., Kocks, U.F., A constitutive description of the deformation of copper based on the use of the mechanical threshold stress as an internal state variable, Ac. Met., 36 (1988) 81-93.

[15] Kocks, U.F., Thermodynamics and kinetics of slip, Prog. Mater. Sci., 19 (1975).

[16] Zeghadi, A., Forest, S., Gourgues, A.-F., Bouaziz, O., Ensemble averaging stress-strain fields in polycrystalline aggregates with a constrained surface microstructure – Part 2: crystal plasticity, Philos. Mag., 87 (2007) 1425-1446.